Thickness-Dependent Photocatalytic Performance of ZnO Nanoplatelets

Changhui Ye,* Yoshio Bando, Guozhen Shen, and Dmitri Golberg

Nanoscale Material Center, National Institute for Materials Science, Namiki 1-1, Tsukuba, Ibaraki 305-0044 Japan

Received: March 27, 2006; In Final Form: May 26, 2006

In this paper, we report the large-scale synthesis of ZnO nanoplatelets as thin as 10 nm. The nanoplatelets show higher efficiency in photodegrading organic dyes than ZnO nanorods do, and for the nanoplatelets, the thinner they are, the higher the performance. The photocatalytic decomposition of organic dyes (eosin B) by ZnO nanoplatelets compares favorably to the performances of ZnS porous nanoparticles and commercial Degussa P25 titania particles. This finding may have significant implications in the environment remediation and the fabrication of functional nanodevices.

1. Introduction

Wide band gap semiconductors are widely used as effective photocatalysts for the degradation of organic pollutants in water.[1,2] By consideration that photochemical reactions mainly take place on the surface of the catalyst, nanoscale materials are believed to perform much better than their bulk counterparts in photocatalytic properties due to the higher surface-to-volume ratio.[1,2] The most extensively studied material is TiO_2, which is particularly good for degrading organic dyes in wastewater due to its peculiar photocatalytic properties.[3] ZnO, a wide band gap semiconductor, is another widely used material for the photocatalytic degradation of organic dyes. The nanoparticles of ZnO perform even better under acidic conditions (for example, pH = 2) in degrading methyl red than TiO_2 nanoparticles do.[4] It has also been shown that ZnO colloids were more effective in production of H_2O_2 and photodegradation of organic acids than TiO_2 colloids.[4] However, nanoparticles with a high surface-to-volume ratio have the tendency to aggregate during aging; henceforth, the active surface area decreases dramatically. It is thus not surprising to note that TiO_2 nanoparticles demonstrate maximal photocatalytic performance only at low annealing temperatures and perform much less efficiently after high-temperature annealing due to the overdue aggregation.[1,5] To overcome this inherent disadvantage, wide band gap semiconductors with various morphologies other than the spherical one have been synthesized and examined with respect to their photocatalytic properties. Recently, Hu et al. reported the higher photocatalytic efficiency of nanoporous ZnS nanoparticles than nonporous ones and suggested that the former have larger surface area than the latter which underwent aggregation.[6]

It is apparent that nanomaterials, which are stable against overdue aggregation and possess a higher surface-to-volume ratio, are the prerequisite for highly efficient photocatalytic degradation of organic pollutants in wastewater. In addition, the fundamental requirement of the band gap value and band positions should be kept in mind. It is well known that ZnO exhibits the richest range of morphologies among the wide band gap semiconductors. It is one of the most reliable materials for the successful synthesis of nanostructures, including nanowires, nanotubes, nanobelts, nanosaw, nanowalls, nanomultipods, nanorings, nanocages, nanohelixes, nanopropellers, and so on.[7] All these morphologies, quite distinct from nanoparticles, still have a high surface-to-volume ratio and are much more stable against aggregation than nanoparticles are; thus, if produced in large scale, they will be particularly useful in environmental protection applications.

In this article, we report on the wafer scale production of single crystalline ZnO nanoplatelets that grow vertically on polycrystalline Al substrates. The thickness of the nanoplatelets could be decreased down to as small as about 10 nm. They grew intertwined and upstanding on the substrates without further aggregation under handling or annealing. The thickness of 10 nm is close to the regime where quantum size effect is prominent. It is well known that band positions will move and higher redox potentials of the free electrons and holes will be achieved accordingly in this regime, which in turn enhances the charge-transfer rates in the materials. Thus a better photocatalytic performance is anticipated even though long-lived emissive states may exist.[1] The increase in the charge transfer rates drastically reduces the direct recombination rate of the charge carriers, which may explain the fact that the nanoplatelets in the present study show very weak photoluminescence under 325-nm excitation, much weaker than ZnO nanorods do (as shown in the following section).

2. Results and Discussion

2.1. Synthesis and Characterization. The ZnO nanoplatelets were synthesized by an aqueous solution growth (ASG) method. A polycrystalline Al wafer (2×2 cm^2) was used as the substrate. The product is uniformly distributed on the whole substrate, as shown in the scanning electron microscopy (SEM) image (Figure 1a). Parts b−d of Figure 1 reveal the platelet morphology in the product. The nanoplatelets grew vertically on the substrate and formed an intertwined pattern. The thickness of the nanoplatelets can be tuned by varying the pH values of the solution as described in the Experimental section. The thickness of 10 nm or smaller can be readily achieved. As shown in the images, nanoplatelets I, II, and III with the thickness approximately 20−50, 15−20, and 10 nm were prepared with adjusting pH values to 6, 9, and 12, respectively. As for a

* To whom correspondence should be addressed. Fax: (+81) 29-851-6280. E-mail: YE.Changhui@nims.go.jp.

10.1021/jp061874w CCC: $33.50
Published on Web 07/14/2006

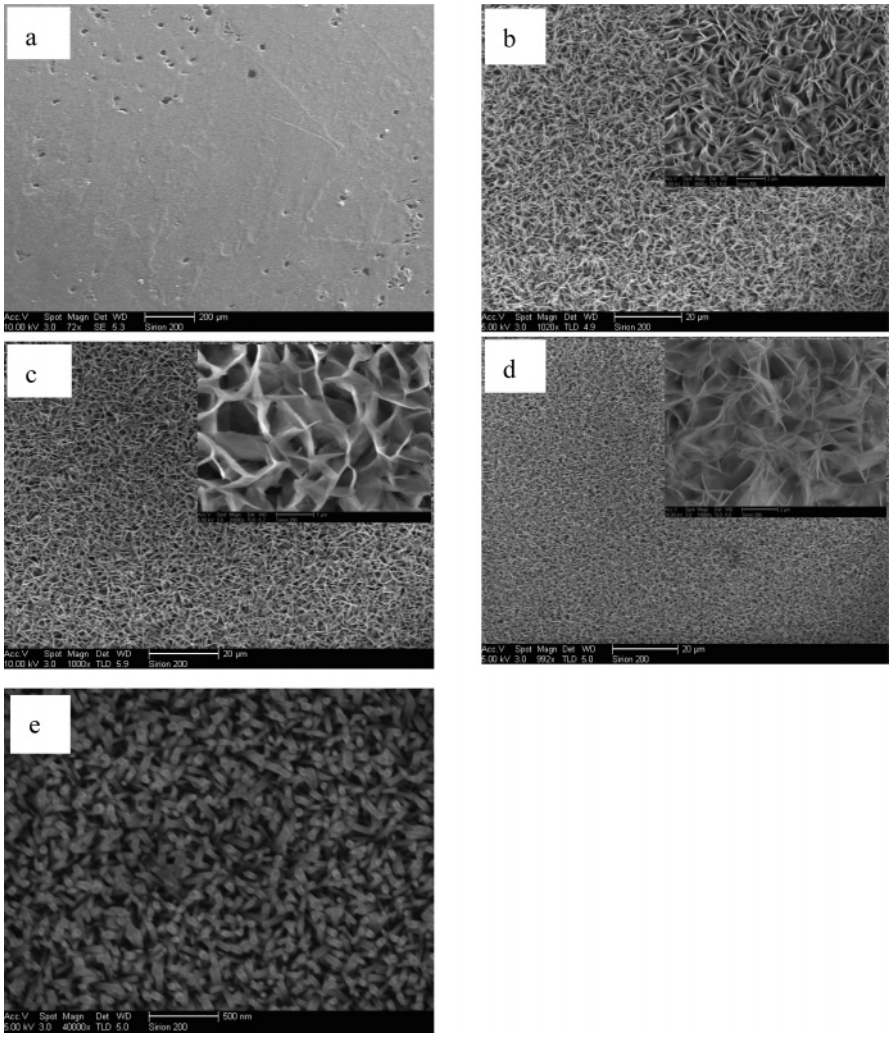

Figure 1. SEM images of the ZnO nanoplatelets at low magnifications (a), nanoplatelets I (b), nanoplatelets II (c), and nanoplatelets III (d), at high magnification, respectively. The insets show the higher magnification view of the nanoplatelets. (e) SEM image of ZnO nanorod arrays.

comparison, the ZnO nanorod arrays on a silicon wafer are displayed in Figure 1e. The nanorods have typical diameter of ~60 nm, the length of several micrometers.

The crystal structure of ZnO nanoplatelet III, the thinnest one, was characterized with X-ray diffraction (XRD). Figure 2a shows the XRD pattern of ZnO nanoplatelets III. It is quite striking that the XRD pattern demonstrates a much stronger (100) peak than the (002) peak, completely different from that for the ZnO nanorod arrays (Figure 2b). The intensity ratio of (100) to (002) peaks for the nanoplatelets is also much larger than that for the bulk ZnO, thus implying the preferred orientation of the nanoplatelets perpendicular to the *c* axis.

To further investigate the morphology and the structure of the ZnO nanoplatelets, transmission electron microscopy (TEM) and high-resolution transmission electron microscopy (HRTEM) were employed. The TEM image of a ZnO nanoplatelet III is shown in Figure 3a, from which it is clear that the nanoplatelet is very thin, with the morphology like a piece of silk. The selected electron diffraction (SAED) pattern in the inset taken along the [0001] zone axis demonstrates the crystalline nature of the nanoplatelet. It also reveals that the top and bottom wide surfaces of the nanoplatelet are ±(0001) planes. The HRTEM image in Figure 3b shows the lattice fringes corresponding to the $\{10\bar{1}0\}$ planes. The energy dispersive spectroscopy (EDS) spectrum in Figure 3c indicates that the nanoplatelet is composed of Zn, O, and Al elements. The signals of Cu and C come from the carbon-coated copper grid. The EDS spectrum indicates that the nanoplatelets are made of Al-doped ZnO. The doping is believed to relate to the growth process, where the $Al(OH)_4^-$ species played a significant role in the formation of the ±(0001) surface dominated thin nanoplatelets as discussed in next section.

The growth of thin ZnO nanoplatelets is mediated by the adsorption of $Al(OH)_4^-$ ions. As known, Al undergoes chemical reactions under alkaline conditions in the presence of amine (hexamethyltetramine) that result in $Al(OH)_4^-$, which could presumably bind to the positively charged Zn^{2+}-terminated (0001) surface (which is a polar surface) of ZnO more strongly than to other nonpolar surfaces and effectively blocking the growth along the [0001] direction. This allows the lateral growth to occur. Thin nanoplatelets, similar to the organic additive mediated growth of (0001) surface dominated ZnO nanostructures, thus form.[8,9] The thickness of the nanoplatelets could be adjusted by the adsorption quantity and coverage rate of the $Al(OH)_4^-$ ions on the (0001) surface planes, which could in turn be tuned by changing the pH values of the solution. With an increase in the pH values, the concentration of $Al(OH)_4^-$ ions also increases, and the increase of the adsorption quantity and coverage rate of the $Al(OH)_4^-$ ions on the (0001) surface planes causes the decrease in the nanoplatelet thickness.

2.2. Photocatalytic Performance. The as-produced ZnO nanoplatelets has been investigated for the applicability in photodegrading organic dyes of eosin B, methyl orange, and methyl red. Parts a−c of Figure 4 show the absorption spectra of aqueous solutions of eosin B, methyl orange, and methyl

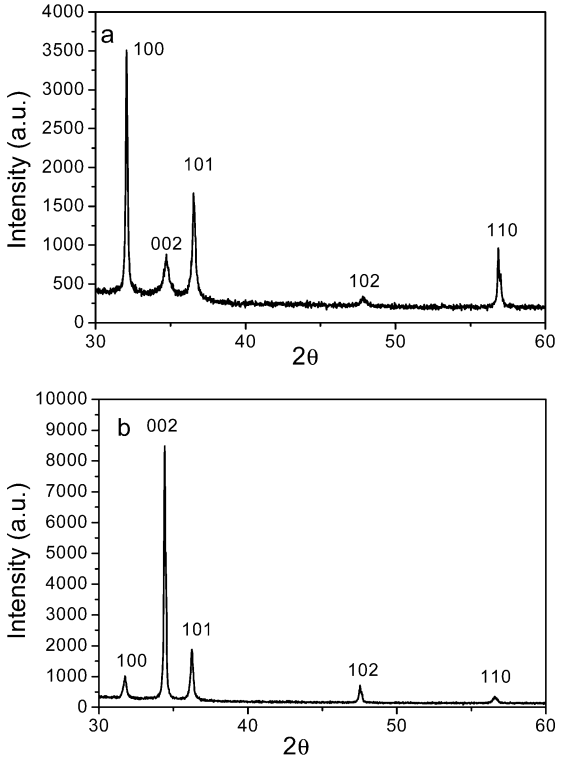

Figure 2. XRD pattern of the ZnO nanoplatelets (a) and nanorods (b). All the diffraction peaks can be readily indexed to the hexagonal phase of ZnO.

red (initial concentration of 1.0×10^{-5} M, 30 mL), respectively, in the presence of the ZnO nanoplatelets III (2 mg) under exposure to UV light for a different period of time. As shown in Figure 4a, the absorption peak corresponding to the eosin B molecules at 517 nm decreases in intensity rapidly with the extension of the exposure time, and disappears almost completely after ~30 min. No new absorption peaks appear in the whole spectrum. In parts b and c of Figure 4, the similar trends have been observed for the photodegradation of methyl orange and methyl red; however, the photodegradation efficiency for the latter two cases is lower than the former one, with the degradation time of methyl orange and methyl red of ~60 and ~75 min, respectively. The exact processes of the degradation of the organic dyes to small molecules and free radicals by the nanoplatelets are, however, not yet clear.

The decomposition kinetics is understood according to physical chemistry principles, and the results are displayed in Figure 5. In these figures, the solid squares are the experimental data, and the solid lines are fitting curves using the exponential decay formula $Y(t) = Y(0)\exp(-kt)$, where $Y(t)$ is the relative concentration of the organic dyes in the solution at time t, $Y(0)$ is the initial relative concentration, namely, 100%, and k is the photodegradation rate constant. This decay behavior can be derived from the first-order reaction kinetics. For a simple reaction such as A → B + C + ..., the change of the concentration of A is $d[\mathrm{A}]/dt = -k[A]$ for the first-order reaction kinetics. From this equation, one can get $[\mathrm{A}(t)] = [\mathrm{A}(0)]\exp(-kt)$ under the conditions of $\mathrm{A}(\infty) \rightarrow 0$. Divided by the initial concentration A(0), this equation is the same to the above exponential decay formula. From the fitting, we find that the photodegradation of these three organic dyes all follows the first-order kinetics. The rate constants of the degradation reactions for eosin B, methyl orange, and methyl red are $(3.1 \pm 0.4) \times 10^{-3}$, $(1.5 \pm 0.2) \times 10^{-3}$, and $(1.1 \pm 0.2) \times 10^{-3}$ s^{-1}, respectively.

A further comparative experiment was carried out to investigate the photocatalytic activity of the ZnO nanoplatelets. The solution of eosin B experienced a series of experimental conditions: (a) with ZnO nanoplatelets III (2 mg), in the dark; (b) without catalyst, with UV light; (c) with ZnO nanorods (2 mg) and UV light; (d) with ZnO nanoplatelets I (2 mg) and V light; (e) with ZnO nanoplatelets II (2 mg) and UV light; (f) with ZnO nanoplatelets III (2 mg) and UV light. The results are illustrated in Figure 6. Under the experimental conditions of a and b, the photocatalytic effect on eosin degradation without catalysts or without exposure to UV light is similarly low, where only a slight decrease in the concentration of eosin B was detected. However, from the data in curves c (ZnO nanorods), d (ZnO nanoplatelets I), e (ZnO nanoplatelets II), and f (ZnO nanoplatelets III), it is apparent that under identical conditions with exposure to UV light, the ZnO nanoplatelets demonstrate much greater photocatalytic activity in degradating eosin B than ZnO nanorods do, in agreement with Tian et al suggested.[9] It is worth noting that the thinner nanoplatelets become, the higher their performance. Such trend in the photocatalytic activity of the ZnO nanomaterials is in line with the higher surface-to-volume ratio of the nanoplatelets than the nanorods and the thinner nanoplatelets compared to the thicker ones. It is also noteworthy that there is another possibility to account for the better performance in the photocatalytic activity of the ZnO nanoplatelets than the ZnO nanorods. The photocatalytic efficiency is surface plane dependent. It has been demonstrated that Pt nanocrystals show a surface plane dependent catalytic ability.[10] From the structural point of view, the ±(1000) planes of ZnO are polar ones. They possibly adsorb the organic dyes more strongly than other nonpolar planes such as the {1010} planes in the nanorods and nanoparticles. Since organic dyes could be degraded only if they adsorb on the surface of the catalyst, the ±(1000) planes of ZnO may dominate, to some extent, the photochemical processes in degrading the organic dyes. This surmise will be examined elsewhere. The photodegradation of eosin B, methyl orange, and methyl red by ZnO nanoplatelets follows first-order kinetics with a different rate constant. However, the carrier charge-transfer processes and reactions are still not clear, and free radicals of various species may be involved in the photochemical reactions,[1,6] which entails further investigation.

Moreover, we also analyzed the photocatalytic degradation of eosin B by ZnS porous nanoparticles and Degussa P25 titania.[6] We notice that the performance of the ZnO nanoplatelets is much better than commercial Degussa P25 titania, and the thinnest nanoplatelets perform better than to the porous ZnS nanoparticles.

2.3. Photoluminescence. The photoluminescence properties of the nanorods and the nanoplatelets are characterized at room temperature, and the curves are displayed in Figure 7. It is clear from the figure that the nanorods emit a much stronger UV light (~380 nm), whereas the nanoplatelets emit weak UV and visible light, which is a consequence of the larger surface area of the nanoplatelets.

3. Conclusions

In conclusion, ZnO nanoplatelets with a tunable thickness (as thin as about 10 nm) have been produced in a wafer scale on polycrystalline Al substrates. The formation of the thin nanoplatelets was mediated by the $Al(OH)_4^-$ ions. The nanoplatelets are dominated by the ±(0001) surface planes. Photodegradation of eosin B, methyl orange, and methyl red have been demonstrated. The photodegradation of eosin B is more

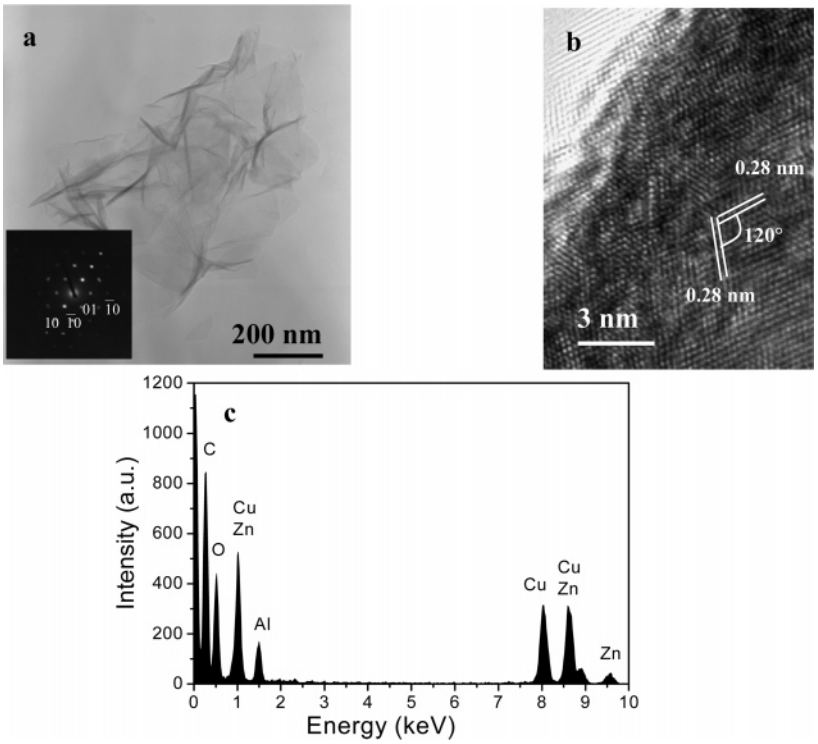

Figure 3. (a) TEM image of one ZnO nanoplatelet III. The inset is an SAED pattern recorded along the [0001] zone axis. (b) HRTEM image of the same nanoplatelet. The lattice fringes correspond to the $(10\bar{1}0)$ lattice planes. (c) EDS spectrum of this nanoplatelet.

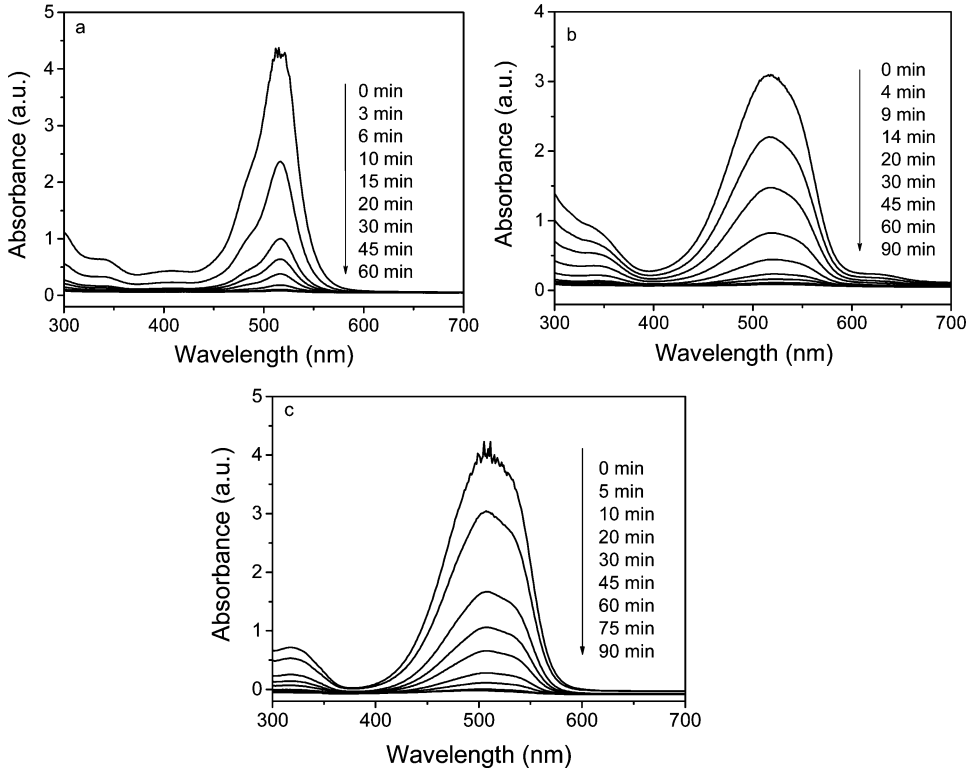

Figure 4. Absorption spectra of solutions of (a) eosin B (1.0×10^{-5} M, 30 mL), (b) methyl orange (1.0×10^{-5} M, 30 mL), and (c) methyl red (1.0×10^{-5} M, 30 mL) in the presence of the ZnO nanoplatelets III (2 mg) under exposure to UV light.

efficient by ZnO nanoplatelets than by ZnO nanorods. The thinner the nanoplatelets, the higher their performance. This may be explained based the surface area's criteria. The excellent performance of ZnO nanoplatelets in photodegrading organic dyes is significant for the environmental remediation and photocatalysis applications.

4. Experimental Section

All chemicals were used as received without further purification.

Growth of ZnO Nanoplatelets. Polycrystalline aluminum substrates (2×2 cm^2) were cleaned in acetone in a sonication bath, cleaned with deionized water, and dried at room temper-

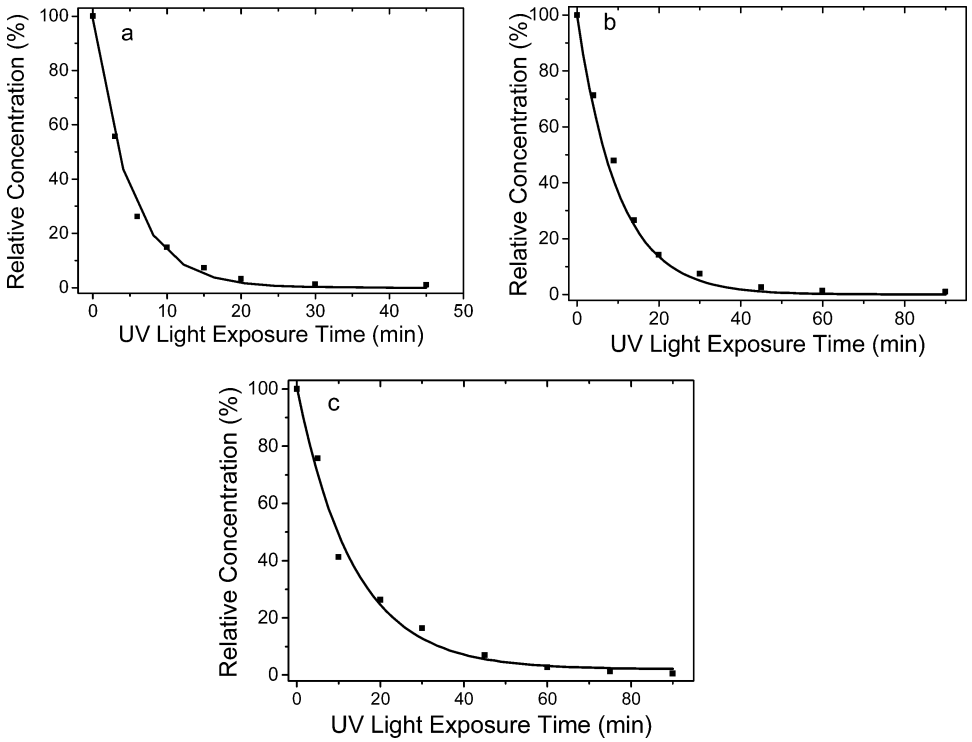

Figure 5. Apparent photodegradation kinetics of eosin B (a), methyl orange (b), and methyl red (c), respectively.

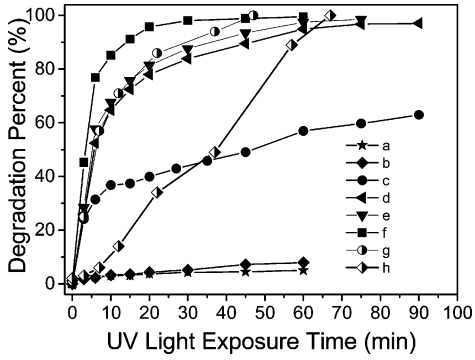

Figure 6. Photodegradation of eosin B (1.0×10^{-5} M, 30 mL) under different conditions: (a) with ZnO nanoplatelets (2 mg), in the dark; (b) without catalyst, with UV light; (c) with ZnO nanorods (2 mg) and UV light; (d) with ZnO nanoplatelets I (2 mg) and V light; (e) with ZnO nanoplatelets II (2 mg) and UV light; (f) with ZnO nanoplatelets III (2 mg) and UV light; (g) with porous ZnS nanoparticles (10 mg) and UV light; (h) with Degussa P25 titania (10 mg) and UV light. (Data g and h are cited from ref 6).

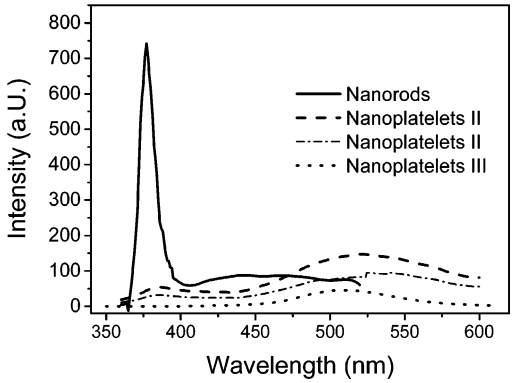

Figure 7. Photoluminescence spectra of ZnO nanoplatelets and nanorods. The emission spectra were recorded with excitation wavelength of 325 nm.

ature. The substrates were placed upside down in a solution containing 0.02 M $Zn(NO_3)_2 \cdot 6H_2O$ and 0.02 M hexamethyltetramine and reacted at 90 °C for different time durations ranging from 30 min to 18 h. The pH values of the solution were adjusted with the addition of $NH_3 \cdot H_2O$. Nanoplatelets I, II, and III were prepared with pH values of 6, 9, and 12, respectively.

Growth of ZnO Nanorods. Single crystalline silicon wafers were cleaned similarly. Substrates were coated with zinc acetate dihydrate solution in ethanol with different concentrations and coating rounds, which yielded ZnO seed crystals with different density and aggregation status after annealing in air at 350 °C. The substrates were placed upside down in a solution containing 0.02 M $Zn(NO_3)_2 \cdot 6H_2O$ and 0.02 M hexamethyltetramine and reacted at 90 °C for different time durations ranging from 30 min to 18 h.[11]

Characterization. XRD (RINT 2200, Cu Kα, $\lambda = 0.15418$ nm) patterns and SEM (JSM-6700F) images were obtained for the as-grown samples. TEM and HRTEM (JEM 3000F, 300 kV) images and EDS spectra were obtained. The samples were sonicated for several minutes in ethanol and several drops of the solution were dripped on the carbon coated copper grids.

Photocatalytic Activity Measurements. UV−vis absorption spectra of the samples were recorded using a spectrophotometer (CARY-5E). The organic dyes and the catalyst were magnetically stirred thoroughly in the dark to reach the adsorption equilibrium of the organic dyes with the catalyst and then exposed to light from a UV light source (300 W, distance of 6 cm). Before recording the absorption spectra, the solution was bubbled with argon gas for 20 min to decrease the dissolution content of oxygen gas. The absorption spectra were recorded at different intervals to monitor the photodegradation process. The ZnO nanoplatelets were weighted as follows. Generally, due to the very small thickness and low density of the nanoplatelets on the aluminum substrate, several substrates with the nanoplatelets were weighed before and after scraping with a knife, until 20 mg nanoplatelets have been scraped off. The 20 mg nanoplatelets were dispersed in deionized water and

stirred magnetically. Then, 10 vol % (close to 2 mg nanoplatelets included) was used for the photocatalytic measurement.

A room-temperature photoluminescence spectrum was recorded with an Edinburgh luminescence spectrometer (FLS 920) using a xenon lamp (900) as the excitation source with the excitation wavelength of 325 nm.

Acknowledgment. This work was supported by the Japan Society for the Promotion of Science (JSPS) (Fellowship tenable at the National Institute for Materials Science, Tsukuba, Japan). C.Y. thanks JSPS for the fellowship.

References and Notes

(1) Hoffmann, M. R.; Martin, S. T.; Choi, W.; Bahnemann, D. W. *Chem. Rev.* **1995**, *95*, 69−96.

(2) (a) Lewis, L. N. *Chem. Rev.* **1993**, *93*, 2693−2730. (b) Nedeljkovic, J. M.; Nenadovic, M. T.; Micic, O. I.; Nozic, A. J. *J. Phys. Chem.* **1986**, *90*, 12−13.

(3) (a) Linsebigler, A. L.; Lu, G.; Yates, J. T. *Chem. Rev.* **1995**, *95*, 735−758. (b) Martin, S. T.; Lee, A. T.; Hoffmann, M. R. *Environ. Sci. Technol.* **1995**, *29*, 2567−2573.

(4) (a) Curri, M. L.; Comparelli, R.; Cozzoli, P. D.; Mascolo, G.; Agostiano, A. *Mater. Sci. Eng. C* **2003**, *23*, 285−289. (b) Hoffman, A. J.; Carraway, E. R.; Hoffmann, M. R. *Environ. Sci. Technol.* **1994**, *28*, 776−785. (c) Carraway, E. R.; Hoffman, A. J.; Hoffmann, M. R. *Environ. Sci. Technol.* **1994**, *28*, 786−793.

(5) Tunesi, S.; Anderson, M. *J. Phys. Chem.* **1991**, *95*, 3399−3405.

(6) Hu, J.; Ren, L.; Guo, Y.; Liang, H.; Cao, A.; Wan, L.; Bai, C. *Angew. Chem., Int. Ed.* **2005**, *44*, 1269−1273.

(7) (a) Wang, Z. L. *J. Phys. Condens. Matter* **2004**, *16*, R829−R858. (b) Ye, C. H.; Fang, X. S.; Hao, Y. F.; Teng, X. M.; Zhang, L. D. *J. Phys. Chem. B* **2005**, *109*, 19758−19765. (c) Shen, G. Z.; Bando, Y.; Liu, B. D.; Golberg, D.; Lee, C. J. *Adv. Funct. Mater.* **2006**, *16*, 410−416.

(8) Koh, Y. W.; Lin, M.; Tan, C. K.; Foo, Y. L.; Loh, K. P. *J. Phys. Chem. B.* **2004**, *108*, 11419−11425.

(9) Tian, Z. R.; Voigt, J. A.; Liu, J.; Mckenzie, B.; Mcdermott, M. J.; Rodriguez, M. A.; Konishi, H.;Xu, H. F. *Nat. Mater.* **2003**, *2*, 821−826.

(10) Narayanan, R.; El-Sayed, M. A. *Nano Lett.* **2004**, *4*, 1343−1348.

(11) (a) Govender, K.; Boyle, D. S.; O'Brien, P.; Binks, D.; West, D.; Coleman, D. *Adv. Mater.* **2002**, *14*, 1221−1224. (b) Vayssieres, L. *Adv. Mater.* **2003**, *15*, 464−466. (c) Choy, J. H.; Jang, E. S.; Won, J. H.; Chung, J. H.; Jang, D. J.; Kim, Y. W. *Adv. Mater.* **2003**, *15*, 1911−1914. (d) Greene, L. E.; Law, M.; Goldberger, J.; Kim, F.; Johnson, J. C.; Zhang, Y.; Saykally, R. J.; Yang, P. *Angew. Chem., Int. Ed.* **2003**, *42*, 3031−3034. (e) Greene, L. E.; Law, M.; Tan, D. H.; Montano, M.; Goldberger, J.; Somorjai, G.; Yang, P. *Nano Lett.* **2005**, *5*, 1231−1236.